Inorganica Chimica Acta 372 (2011) 191–199

Contents lists available at ScienceDirect

Inorganica Chimica Acta

journal homepage: www.elsevier.com/locate/ica

3,5-Lutidine coordinated zinc(II) aryl carboxylate complexes: Precursors for zinc(II) oxide

Umesh Kumar [a], Jency Thomas [b], Rajamani Nagarajan [a], Natesan Thirupathi [a,*]

[a] Department of Chemistry, University of Delhi, Delhi 110007, India
[b] Department of Chemistry, Indian Institute of Technology Delhi, Delhi 110016, India

ARTICLE INFO

Article history:
Available online 3 February 2011

This article is dedicated to Prof. S.S. Krishnamurthy on the occasion of his 70th birthday.

Keywords:
Zinc(II) aryl carboxylates
3,5-Lutidine
Acetate exchange reaction
Thermal decomposition studies
ZnO

ABSTRACT

The reaction of $Zn(\kappa^2O,O'–OAc)_2{\cdot}2H_2O$ with two equiv of 3,5-lutidine in methanol at room temperature for 12 h afforded $[Zn(OAc)_2(3,5\text{-lutidine})_2]{\cdot}\ H_2O$ (**1**) in 91% yield. The acetate exchange reaction of **1** with two equiv of aryl carboxylic acids in methanol at room temperature for 12 h afforded $[Zn(\mu_2\text{-}\kappa^1O{:}\kappa^1O'–O_2CAr)_2(3,5\text{-lutidine})]_2$ [Ar = C_6H_5 (**2**) and C_6H_4Me-3 (**3**)], $[Zn(OC(O)C_6H_4Me\text{-}2)_2(3,5\text{-lutidine})_2]$ (**4**) and $[Zn(\kappa^2O,O'–O_2CC_6H_4Me\text{-}4)_2(3,5\text{-lutidine})_2]$ (**5**) in ⩾90% yield. Complexes **1**–**5** were characterized by microanalytical, IR, solution (^1H and ^{13}C) and solid-state cross-polarization magic angle spinning ^{13}C NMR and X-ray diffraction data. The zinc atom in **1** is surrounded by nitrogen atom of two 3,5-lutidine and oxygen atom of two monodentate acetate moiety and thus attains a tetrahedral geometry. One of the acetate moieties is hydrogen bonded with a water molecule in the crystal lattice. Complexes **2** and **3** possess a dinuclear paddlewheel framework with a square pyramidal geometry around the zinc atom whereas **4** and **5** are mononuclear species with the zinc atom in tetrahedral and an octahedral geometry, respectively. Thermogravimetric analyses of **2**–**5** suggested ZnO as the decomposed product followed by the confirmation from the powder X-ray diffraction patterns. Enormous gas evolution resulting in porous ZnO during thermal decomposition was evidenced from scanning electron microscopic images.

1. Introduction

ZnO is one of the useful materials in photonics, electronics, optoelectronics, information storage, photography, catalysis, biological and chemical sensing [1,2]. Several synthetic routes are known for ZnO powder such as sol–gel method [3,4], pyrolysis of chelate complexes [5], spray pyrolysis [6], and thermal decomposition of precursors [7]. Organometallic precursors such as diethyl zinc [8–10], dicyclohexyl zinc [11], and dimethylzinc [12] were also used as precursors for nano-sized ZnO. The dialkylzinc precursors are pyrophoric and hence extra precautions need to be taken in handling these precursors. Hence, there exists a need to synthesize air stable and safe to handle zinc containing precursors that can easily result in the formation of ZnO. Few zinc ketoiminato complexes [13,14] as well as few Lewis base coordinated zinc(II) carboxylate complexes [15–17] were also reported to be useful precursors for ZnO .

Lewis base coordinated zinc(II) carboxylate complexes constitute an important class of coordination compounds due to their relevance as structural and functional model for biologically important metalloenzymes [18–23], as Lewis acid catalysts for the copolymerization of cyclohexene oxide and CO_2 to afford polycarbonates [24–26], and as secondary building units (SBUs) of the carboxylate based metal organic frameworks (MOFs) [27–34]. The nuclearity and carboxylate coordination modes in Lewis base coordinated zinc(II) aryl carboxylate complexes were shown to depend upon the method of preparation, nature of carboxylate moiety, Lewis base, the ratio of reactants and other reaction conditions [17,35–39].

Recently, we have isolated a series Lewis base coordinated zinc(II) acetate and zinc(II) pivalate complexes with di and trinuclear core as well as a one dimensional coordination polymer from the condensation reaction involving $Zn(\kappa^2O,O'–OAc)_2{\cdot}2H_2O$ (or) $Zn(O_2C^tBu)_2$ and Lewis bases in methanol at ambient condition [40,41]. From this study, it was concluded that subtle basic/steric properties of Lewis bases and noncovalent interactions in the crystal lattice influence the nuclearity and carboxylate coordination modes of the products. Further, such complexes upon thermolysis lead to the formation of volatile species instead of ZnO as revealed by TGA/DTA studies. In continuation of our work in zinc(II) carboxylate chemistry, we report herein the synthesis, structural aspects of $[Zn(OAc)_2(3,5\text{-lutidine})_2]{\cdot}H_2O$ (**1**) and 3,5-lutidine coordinated zinc(II) aryl carboxylate complexes **2**–**5** shown in Chart 1. These

* Corresponding author. Tel.: +91 (0) 11 2766 6646x189; fax: +91 (0) 11 2766 6605.
E-mail addresses: tnat@chemistry.du.ac.in, thirupathi_n@yahoo.com (N. Thirupathi).

0020-1693/$ - see front matter © 2011 Elsevier B.V. All rights reserved.
doi:10.1016/j.ica.2011.01.083

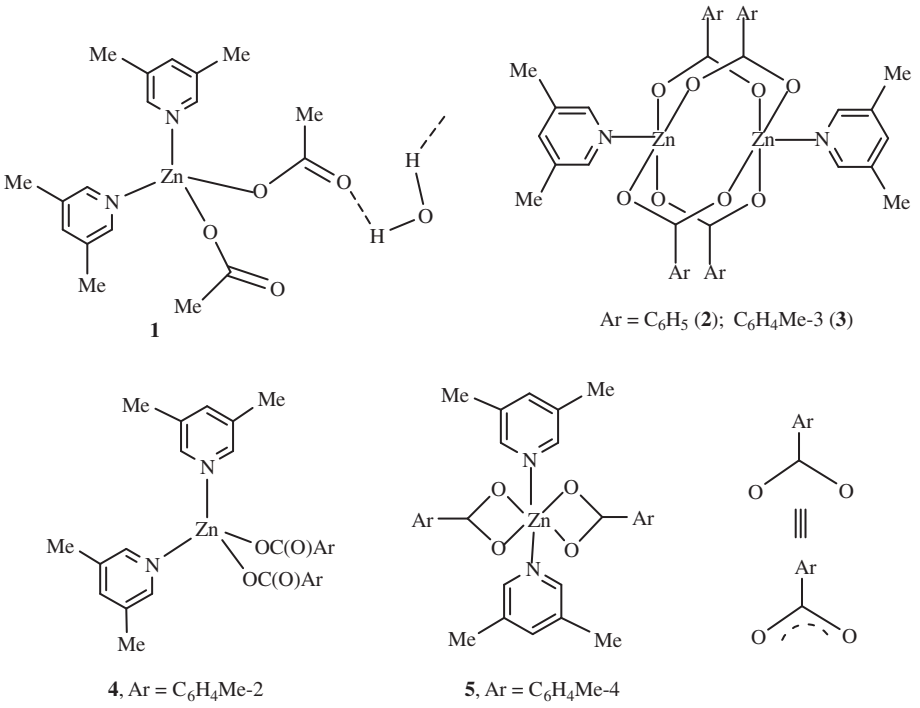

1

Ar = C_6H_5 (**2**); C_6H_4Me-3 (**3**)

4, Ar = C_6H_4Me-2

5, Ar = C_6H_4Me-4

Chart 1.

complexes upon thermolysis afforded porous ZnO as confirmed by powder X-ray diffraction data and scanning electron microscopic images.

2. Experimental

2.1. Materials and methods

Zn(κ^2*O*,*O*′–OAc)$_2$·2H$_2$O, 3,5-lutidine, benzoic acid, *o*-toluic acid, *m*-toluic acid and *p*-toluic acid were purchased from commercial sources and used as received. Elemental analyses were performed on an Elementar Analysensysteme GmbH VarioEL V3.00. The IR spectral data were obtained on a Shimadzu IR435 spectrometer using KBr pellet in the frequency range 400–4000 cm^{-1}. ^{1}H and ^{13}C NMR spectra were recorded on an Avance Bruker-300 NMR spectrometer operating at field strengths of 300 and 75·5 MHz, respectively and chemical shifts are reported relative to tetramethylsilane (TMS) or residual solvent signal. The solid-state cross-polarization magic angle spinning (CP-MAS) ^{13}C NMR spectra were recorded on a DSX-300 MHz spectrometer and the chemical shifts were referenced with respect to TMS. TOF-MS spectra were recorded on a Micromass LCT KC 455 instrument using electrospray positive ion mode. The thermal analyses (TGA/DTA) were carried out on a combined TGA/DTA Shimadzu (model TA-60WS) instrument at a heating rate of 10 °C/min. Powder X-ray diffraction (PXRD) patterns were recorded on Philips Xpert and Bruker D8 Advance instruments. The scanning electron microscopic (SEM) images were obtained using Hitachi 7500 as well as FEI Quanta 200F microscopes. The reported yield of **1** is based on Zn(κ^2*O*,*O*′–OAc)$_2$·2H$_2$O and those of **2**–**5** are based on **1**.

2.2. [Zn(OAc)$_2$(3,5-lutidine)$_2$]·H$_2$O (*1*)

Zn(κ^2*O*,*O*′–OAc)$_2$·2H$_2$O (2.00 g, 9.11 mmol) was dissolved in methanol (70 mL). To the aforementioned solution, 3,5-lutidine (2.00 g, 18.68 mmol) in methanol (10 mL) was added drop wise and the resulting solution was stirred at room temperature for 12 h. The reaction mixture was concentrated under vacuum to *ca.* 20 mL and left at room temperature for several hours to afford **1** as colorless crystals. Crystals were separated and washed with cold *n*-hexane to afford **1** in 91% yield (3.45 g, 8.30 mmol). FT-IR (KBr, cm^{-1}): 3434 (br) for υ(H$_2$O), 1618 (sh), 1603 (vs) for υ_{asym}(O-CO), 1399 (vs) for υ_{sym}(OCO). ^{1}H NMR ($CDCl_3$, 300 MHz, δ ppm): 2.09 (s, 6H, OC(O)C*H*$_3$), 2.33 (s, 12H, NC$_5$H$_3$(C*H*$_3$)$_2$-3,5), 7.45 (s, 2H, *4H* NC$_5$*H*$_3$(CH$_3$)$_2$-3,5), 8.35 (s, 4H, 2*H* & 6*H* NC$_5$*H*$_3$(CH$_3$)$_2$-3,5). ^{13}C NMR ($CDCl_3$, 75.5 MHz, δ ppm): 18.0, 22.3 (*C*H$_3$), 133.9, 139.8, 146.7 (NC$_5$H$_3$(CH$_3$)$_2$-3,5), 179.2 (O*C*(O)). MS (TOF, ES$^+$) *m/z* (intensity %): 398 [M–H$_2$O + H]$^+$ (1 0 0). *Anal.* Calc. for C$_{18}$H$_{24}$N$_2$O$_4$Zn·H$_2$O (415.81): C, 52.00; H, 6.30; N, 6.74. Found: C, 52.50; H, 6.47; N, 6.71%.

2.3. [Zn(μ_2-κ^1*O*:κ^1*O*′–O$_2$CC$_6$H$_5$)$_2$(3,5-lutidine)]$_2$ (*2*)

Complex **1** (2.00 g, 4.81 mmol) was dissolved in methanol (60 mL). To the aforementioned solution, benzoic acid (1.26 g, 10.31 mmol) was added pinch wise and the resulting homogeneous solution was stirred at room temperature for 12 h. The volatiles were removed under vacuum to afford colorless solid. The solid was purified by crystallization from methanol/chloroform mixture at room temperature over a period of one week to afford **2** as colorless crystals in quantitative yield (1.99 g, 2.40 mmol). FT-IR (KBr, cm^{-1}): 1641 (s), 1576 (m) for υ_{asym}(OCO), 1459 (m), 1408 (s) for υ_{sym}(OCO). ^{1}H NMR ($CDCl_3$, 300 MHz, δ ppm): 2.29 (s, 12H, NC$_5$H$_3$(C*H*$_3$)$_2$-3,5), 7.30 (t, 8H, *3H & 5H* C$_6$*H*$_5$, J_{HH} = 8.87 Hz), 7.34 (s, 2H, *4H* NC$_5$*H*$_3$(CH$_3$)$_2$-3,5), 7.43 (t, 4H, *4H* C$_6$*H*$_5$, J_{HH} = 7.31 Hz), 8.11 (d, 8H, 2*H* & 6*H* C$_6$*H*$_5$, J_{HH} = 7.49 Hz), 8.51 (s, 4H, 2*H* & 6*H* NC$_5$*H*$_3$(CH$_3$)$_2$-3,5). ^{13}C NMR ($CDCl_3$, 75·5 MHz, δ ppm): 18.2 (*C*H$_3$), 127.5, 130.3, 131.4, 133.6, 134.6, 140.8, 146.5 (Ar*C*), 174.0 (O*C*(O)). MS (TOF, ES$^+$) *m/z* (intensity %): 831 [M+H]$^+$ (8). *Anal.* Calc. for C$_{42}$H$_{38}$N$_2$O$_8$Zn$_2$ (829.55): C, 60.81; H, 4.62; N, 3.38. Found: C, 60.77; H, 4.98; N, 3.38%.

2.4. [Zn(μ_2–κ^1*O*:κ^1*O*′–O$_2$CC$_6$H$_4$Me-3)$_2$(3,5-lutidine)]$_2$ (*3*)

Complex **1** (2.00 g, 4.81 mmol) was dissolved in methanol (60 mL). To the aforementioned solution, *m*-toluic acid (1.40 g,

10.31 mmol) was added pinch wise and the resulting homogeneous solution was stirred at room temperature for 12 h. The volatiles were removed under vacuum to afford colorless solid. The solid was purified by crystallization from chloroform/acetonitrile mixture at room temperature over a period of one week to afford **3** as colorless crystals in 90% yield (1.92 g, 2.16 mmol). FT-IR (KBr, cm^{-1}): 1605 (s), 1583 (s) for υ_{asym}(OCO), 1426 (s), 1400 (vs) for υ_{sym}(OCO). ^{1}H NMR ($CDCl_3$, 300 MHz, δ ppm): 2.29 (s, 12H, $C_6H_4(CH_3)$-3), 2.32 (s, 12H, $NC_5H_3(CH_3)_2$-3,5), 7.22 (m, 4H, *5H* $C_6H_4(CH_3)$-3), 7.25 (d, 4H, *4H* $C_6H_4(CH_3)$-3, J_{HH} = 7.50 Hz), 7.46 (s, 2H, *4H* $NC_5H_3(CH_3)_2$-3,5), 7.92 (d, 4H, 6*H* $C_6H_4(CH_3)$-3, J_{HH} = 10.80 Hz), 7.94 (s, 4H, 2*H* $C_6H_4(CH_3)$-3), 8.50 (s, 4H, 2*H* & 6*H* $NC_5H_3(CH_3)_2$-3,5). ^{13}C NMR ($CDCl_3$, 75·5 MHz, δ ppm): 18.3, 21.2 (CH_3), 127.5, 131.1, 132.2, 133.7, 134.6, 137.2, 140.8, 146.7 (ArC), 174.32 (OC(O)). Note: Only 8 carbon resonances were observed for ArC rather than the expected 9 resonances presumably due to overlapping peaks. MS (TOF, ES^+) *m/z* (intensity %): 886 $[M+H]^+$ (83). *Anal.* Calc. for $C_{46}H_{46}N_2O_8Zn_2$ (885.70): C, 62.38; H, 5.23; N, 3.16. Found: C, 62.21; H, 5.21; N, 3.02%.

2.5. [Zn(OC(O)C_6H_4Me-2)$_2$(3,5-lutidine)$_2$] (**4**)

Complex **1** (2.00 g, 4.81 mmol) was dissolved in methanol (60 mL). To the aforementioned solution, *o*-toluic acid (1.40 g, 10.31 mmol) was added pinch wise and the resulting homogeneous solution was stirred at room temperature for 12 h. The volatiles were removed under vacuum to afford colorless solid. The solid was purified by crystallization from chloroform/acetonitrile mixture at room temperature over a period of one week to afford **4** as colorless crystals in 90% yield (2.38 g, 4.33 mmol). FT-IR (KBr, cm^{-1}): 1637 (vs), 1562 (m) for υ_{asym}(OCO), 1437 (m) and 1402 (s) for υ_{sym}(OCO). ^{1}H NMR ($CDCl_3$, 300 MHz, δ ppm): 2.29 (s, 12H, $NC_5H_3(CH_3)_2$-3,5), 2.57 (s, 6H, $C_6H_4(CH_3)$-2), 7.14 (br, 4H, 3*H* & 5*H* $C_6H_4(CH_3)$-2), 7.26 (t, 2H, *4H* $C_6H_4(CH_3)$-2, J_{HH} = 6.99 Hz), 7.46 (s, 2H, *4H* $NC_5H_3(CH_3)_2$-3,5), 7.95 (d, 2H, 6*H* $C_6H_4(CH_3)$-2, J_{HH} = 7.33 Hz), 8.48 (s, 4H, 2*H* & 6*H* $NC_5H_3(CH_3)_2$-3,5). ^{13}C NMR ($CDCl_3$, 75·5 MHz, δ ppm): 18.4, 21.8 (CH_3), 127.2, 129.9, 130.6, 134.5, 135.2, 138.6, 140.6, 146.9 (ArC), 175.9 (OC(O)). Note: Only 8 carbon resonances were observed for ArC rather than the expected 9 resonances presumably due to overlapping peaks. MS (TOF, ES^+) *m/z* (intensity %): 551 $[M+H]^+$ (5). *Anal.* Calc. for $C_{30}H_{32}N_2O_4Zn$ (549.98): C, 65.52; H, 5.86; N, 5.09. Found: C, 65.26; H, 5.81; N, 4.87%.

2.6. [Zn(κ^2*O,O*′–$O_2CC_6H_4$Me-4)$_2$(3,5-lutidine)$_2$] (**5**)

Complex **1** (2.00 g, 4.81 mmol) was dissolved in methanol (60 mL). To the aforementioned solution, *p*-toluic acid (1.40 g, 10.31 mmol) was added pinch wise and the resulting homogeneous solution was stirred at room temperature for 12 h. The volatiles were removed under vacuum to afford colorless solid. The solid was purified by crystallization from chloroform/acetonitrile mixture at room temperature over a period of one week to afford **5** as colorless crystals in 90% yield (2.62 g, 4.76 mmol). FT-IR (KBr, cm^{-1}): 1544 (s) for υ_{asym}(OCO), 1405 (vs) for υ_{sym}(OCO). ^{1}H NMR ($CDCl_3$, 300 MHz, δ ppm): 2.30 (s, 12H, $NC_5H_3(CH_3)_2$-3,5), 2.37 (s, 6H, $C_6H_4(CH_3)$-4), 7.15 (d, 4H, *3H* & *5H* $C_6H_4(CH_3)$-4, J_{HH} = 7.86 Hz), 7.43 (s, 2H, *4H* $NC_5H_3(CH_3)_2$-3,5), 8.04 (d, 4H, 2*H* & 6*H* $C_6H_4(CH_3)$-4, J_{HH} = 7.93 Hz), 8.45 (s, 4H, 2*H* & 6*H* $NC_5H_3(CH_3)_2$-3,5). ^{13}C NMR ($CDCl_3$, 75·5 MHz, δ ppm): 18.2, 21.4 (CH_3), 128.2, 130.2, 131.7, 134.2, 140.2, 141.0, 146.8 (ArC), 173.7 (OC(O)). MS (TOF, ES^+) *m/z* (intensity %): 550 $[M+H]^+$ (13). *Anal.* Calc. for $C_{30}H_{32}N_2O_4Zn$ (549.98): C, 65.52; H, 5.86; N, 5.09. Found: C, 65.11; H, 5.83; N, 4.98%.

2.7. Crystal structure determinations

X-ray diffraction studies of suitably sized crystals mounted on a capillary were carried out on a BRUKER AXS SMART-APEX diffractometer with a CCD area detector [(Mo Kα) 0.71073 Å, graphite monochromator] [42]. Frames were collected at 100 K for complex **1** and at 298 K for complexes **2**–**5** by ω, ø and 2θ rotation at 10 s per frame with SMART [42]. The measured intensities were reduced to F^2 and corrected for absorption with SADABS [43]. Structure solution, refinement, and data output were carried out with the SHELXTL program [44]. Non-hydrogen atoms were refined anisotropically. C–H hydrogen atoms were placed in geometrically calculated positions by using a riding model. Images were created with the Diamond program [45]. Hydrogen bonding interactions in the crystal lattice were calculated with SHELXTL [44]. The X-ray crystallographic parameters, details of data collection and structure refinement are presented in Table 1.

3. Results and discussion

3.1. Synthesis

Zn(κ^2*O,O*′–OAc)$_2$·2H_2O was treated with 3,5-lutidine in 1:2 mol ratio in methanol at room temperature for 12 h that afforded

Table 1
Crystallographic and experimental data for **1–5**.

	1	**2**	**3**	**4**	**5**
Empirical formula	$C_{18}H_{24}N_2O_5Zn$	$C_{42}H_{38}N_2O_8Zn_2$	$C_{46}H_{46}N_2O_8Zn_2$	$C_{30}H_{32}N_2O_4Zn$	$C_{30}H_{32}N_2O_4Zn$
Formula weight	413.78	829.52	885.63	549.97	549.97
Crystal system	triclinic	triclinic	triclinic	monoclinic	orthorhombic
Space group	$P\bar{1}$	$P\bar{1}$	$P\bar{1}$	$P2_1/n$	*Ibca*
a (Å)	9.727(2)	10.282(2)	10.734(9)	8.227(2)	15.676(5)
b (Å)	10.361(3)	10.700(2)	10.897(9)	36.602(7)	16.656(6)
c (Å)	10.471(2)	10.801(3)	11.359(10)	9.607(2)	21.058(7)
α (°)	92.678(3)	63.411(3)	63.774(14)	90.00	90.00
β (°)	109.155(3)	66.928(3)	81.812(14)	105.191(3)	90.00
γ (°)	103.752(4)	79.322(4)	63.460(13)	90.00	90.00
V (Å^3)	959.3(4)	977.6(4)	1063.8(16)	2792.1(9)	5498(3)
Z	2	1	1	4	8
Density (calcd) (g cm^{-3})	1.433	1.409	1.382	1.308	1.329
T (*K*)	100(2)	298(2)	298(2)	298(2)	298(2)
λ (Mo Kα) (Å)	0.71073	0.71073	0.71073	0.71073	0.71073
μ (Mo Kα) (cm^{-1})	1.310	1.281	1.182	0.916	0.930
R_1, wR_2 [$I > 2\sigma(I)$][a]	0.0497, 0.0547	0.0490, 0.0633	0.0524, 0.0793	0.0575, 0.0712	0.0486, 0.0538
R_1, wR_2 (all data)[a]	0.1443, 0.1549	0.1150, 0.1280	0.1062, 0.1220	0.1383, 0.1498	0.1183, 0.1219

[a] $R_1 = \Sigma||F_o| - |F_c||/\Sigma|F_o|$; $wR_2 = \left[\Sigma w(|F_o| - |F_c|)^2/\Sigma w|F_o|^2\right]^{1/2}$.

$[Zn(OAc)_2(3,5\text{-lutidine})_2]\cdot H_2O$ (**1**) as colorless solid in 91% yield. Complex **1** was treated with two equiv of aryl carboxylic acids shown in Chart 2 in methanol at room temperature for 12 h that afforded complexes **2**–**5** in ⩾90% yield. Our objectives were two fold; to probe the role of subtle steric/basic properties of the aryl carboxylic acids on the nuclearity/carboxylate coordination modes of the products and to use such products as precursors for ZnO.

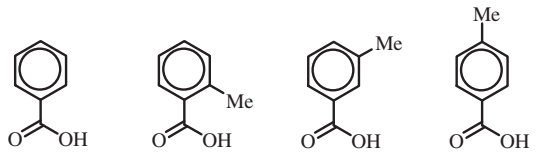

pK_a [46]: 4.20 3.91 4.25 4.37

Chart 2.

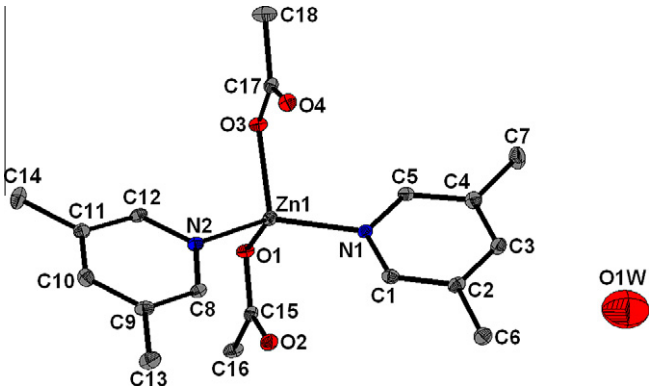

Fig. 1. ORTEP representation of **1** at the 30% probability level. Hydrogen atoms are omitted for clarity.

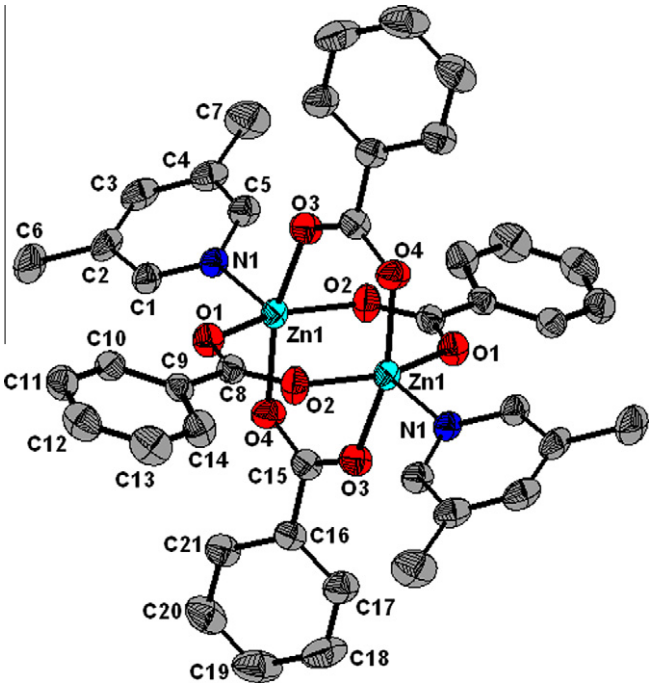

Fig. 2. ORTEP representation of **2** at the 30% probability level. Hydrogen atoms are omitted for clarity.

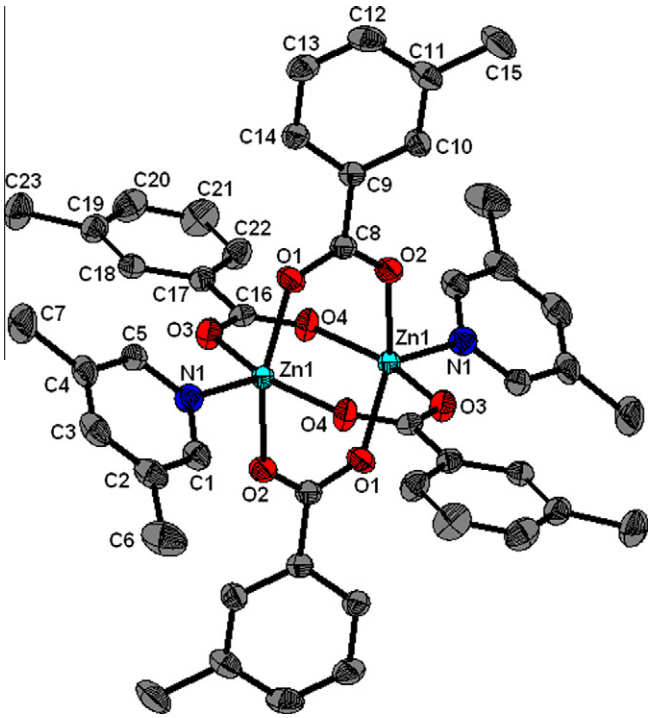

Fig. 3. ORTEP representation of **3** at the 30% probability level. Hydrogen atoms are omitted for clarity.

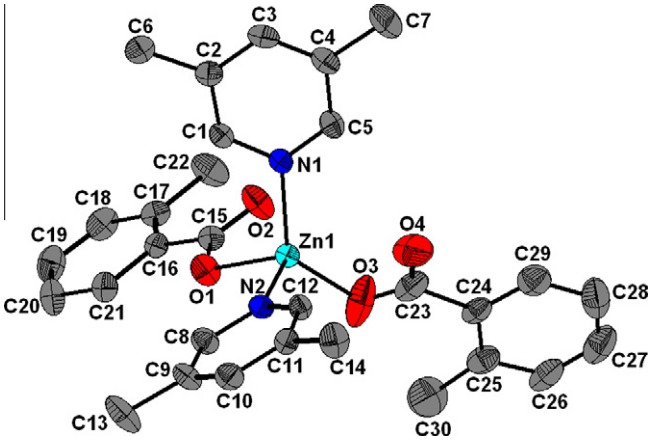

Fig. 4. ORTEP representation of **4** at the 30% probability level. Hydrogen atoms are omitted for clarity.

3.2. Molecular and crystal structures

The molecular structures of **1**–**5** were determined by X-ray diffraction data. The molecular structures of **1**–**5** with atom labeling scheme are shown in Figs. 1–5, respectively. Selected bond parameters for **1**–**5** are listed in Table 2. Complex **1** crystallized as a monohydrate and in this complex the zinc atom surrounded by two oxygen atoms of the monodentate acetate and nitrogen atoms of two 3,5-lutidine and thus attains a tetrahedral geometry. $Zn(OAc)_2(pyridine)_2$ was shown to crystallize in triclinic and tetragonal space groups [47]. The Zn–O [1.981(2) and 1.965(2) Å] and C=O [1.232(5) and 1.235(5) Å] distances are longer but the Zn–N [2.015(3) and 2.041(3) Å] distances are shorter in complex **1** than those observed in $Zn(OAc)_2(pyridine)_2$ [triclinic: Zn–O, 1.945(3) and 1.941(2) Å; C=O, 1.218(4) and 1.218(4) Å; Zn–N, 2.047(2) and 2.076(2) Å]. The bond distance variation may be

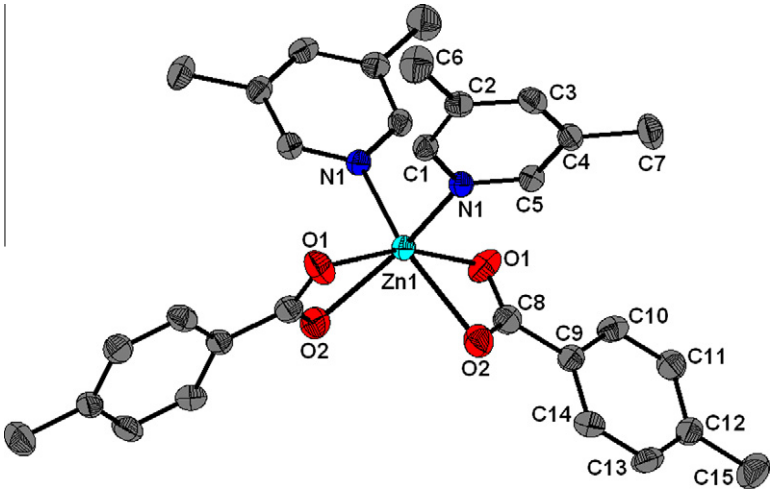

Fig. 5. ORTEP representation of **5** at the 30% probability level. Hydrogen atoms are omitted for clarity.

Table 2
Selected bond lengths (Å) and bond angles (°) for **1**–**5**.

1					
Zn1–O1	1.981(2)	Zn1–O3	1.965(2)	Zn1–N1	2.015(3)
Zn1–N2	2.041(3)	C15–O1	1.299(4)	C15–O2	1.232(5)
C15–C16	1.510(5)	C17–O3	1.286(5)	C17–O4	1.235(5)
C17–C18	1.516(5)	O1–Zn1–O3	99.09(10)	O1–Zn1–N1	110.52(11)
O1–Zn1–N2	105.24(11)	O3–Zn1–N1	106.40(11)	O3–Zn1–N2	105.24(11)
N1–Zn1–N2	126.60(12)	O1–C15–O2	122.7(3)	O3–C17–O4	124.5(3)
	2	**3**		**2**	**3**
Zn1–N1	2.040(2)	2.042(3)	Zn1–O3	2.044(2)	2.029(3)
Zn1–O1	2.024(2)	2.029(3)	Zn1–O4	2.028(2)	2.062(3)
Zn1–O2	2.060(2)	2.040(3)	Zn1···Zn1	2.970(1)	2.965(2)
O2–Zn1–O3	87.35(9)	89.1(1)	O4–Zn1–O1	87.52(9)	88.9(1)
O2–Zn1–O4	88.8(1)	87.6(1)	O2–Zn1–N1	95.41(9)	100.1(1)
O3–Zn1–O4	159.04(9)	159.2(1)	O3–Zn1–N1	99.19(9)	105.1(1)
O2–Zn1–O1	158.79(9)	159.1(1)	O4–Zn1–N1	101.68(9)	95.6(1)
O3–Zn1–O1	88.63(9)	86.9(1)	O1–Zn1–N1	105.79(9)	100.8(1)
4					
Zn1–O1	1.986(3)	Zn1–O3	1.972(4)	Zn1–N1	2.082(3)
Zn1–N2	2.024(2)	C15–O1	1.272(4)	C15–O2	1.218(4)
C15–C16	1.509(5)	C23–O3	1.222(6)	C23–O4	1.250(7)
C23–C24	1.521(6)	O1–Zn1–N1	106.0(1)	O1–Zn1–N2	96.9(1)
O3–Zn1–N1	130.8(2)	O3–Zn1–N2	108.6(2)	O1–C15–O2	121.7(3)
O1–C15–C16	116.1(3)	O2–C15–C16	122.2(3)	O3–C23–O4	122.8(5)
O3–C23–C24	119.8(5)	O4–C23–C24	117.4(6)		
5					
Zn1–O1	2.114(3)	Zn1–O2	2.258(2)	Zn1–N1	2.103(2)
O1–C8	1.255(4)	O2–C8	1.247(4)	C8–C9	1.498(4)
O1–Zn1–O1	160.7(2)	O1–Zn1–O2	105.6(1)	O1–Zn1–N1	98.51(9)
O2–Zn1–N1	153.81(9)	O2–Zn1–O2	90.2(1)	N1–Zn1–N1	95.0(1)
O1–C8–O2	121.0(3)	O1–C8–C9	118.9(3)	O2–C8–C9	120.1(3)

ascribed to higher basicity of 3,5-lutidine (pK_a: 6.15) in the former compared with pyridine (pK_a: 5.23) [46] in $Zn(OAc)_2(pyridine)_2$ and the involvement of C=O oxygen in **1** in intermolecular O–H···O/C–H···O hydrogen bonding in the crystal lattice.

Complexes **2** and **3** consist of a paddlewheel framework wherein the pair of zinc atoms is bridged by four syn–syn bidentate bridging carboxylate moieties. 3,5-lutidine is coordinated to each zinc atom along the non-bonded Zn···Zn axis and thus the zinc atom attains a square pyramidal geometry. It was shown that the non-bonded M···M distance and O–C–O angle in the carboxylate bridged paddlewheel dinuclear complexes depend upon the inductive effect and steric bulk of the substituent on the carbonyl carbon [48]. The molecular structures of several Lewis base coordinated zinc(II) aryl carboxylate complexes with a paddlewheel framework are known [17,35–39,49,50]. The non-bonded Zn···Zn distance, 2.970(1) Å in **2** is slightly longer than that observed in the structurally related $[Zn(\mu_2\text{-}\kappa^1O{:}\kappa^1O'\text{-}O_2CC_6H_5)_2(pyridine)]_2$ (**I**) [2.958(1) Å] [35] indicating the influence of higher basicity of 3,5-lutidine than that of pyridine. The non-bonded Zn···Zn distance in **I**, **2** and **3** [2.965(2) Å] is slightly shorter than that observed in $[Zn(\mu_2\text{-}\kappa^1O{:}\kappa^1O'\text{-}O_2CC_6H_5)_2(quinoxaline)]_2$ (**II**) [2.990(1) Å] [38].

Complex **4** is a mononuclear species with the zinc atom surrounded by oxygen atom of two monodentate *o*-toluate moieties and nitrogen atom of two 3,5-lutidine and the zinc atom thus attains a tetrahedral geometry. The zinc atom in **5** resides on a crystallographic C_2 axis and is surrounded by two oxygen atom of a chelating *p*-toluate and nitrogen atom of 3,5-lutidine and their C_2 symmetry related *p*-toluate and 3,5-lutidine and thus zinc atom attains an octahedral geometry.

Complexes **3**–**5** possess an intermolecular C–H···O interaction in the crystal lattice and such interaction is illustrated in Figs. 6–8, respectively. The O3 atom of the syn–syn bidentate bridging *m*-toluate moiety in **3** forms a C–H···O hydrogen bonding with one of the hydrogen atoms (H23A) bonded to methyl carbon of the *m*-toluate moiety of the inversion related adjacent molecule. The O2 atom of the monodentate *o*-toluate in **4** is involved in a bifurcated intermolecular C–H···O hydrogen bonding with H20 of the *o*-toluate moiety of the translation related adjacent molecule and the other with H6C of 3,5-lutidine of the inversion related adjacent molecule. The O1 atom of the chelating *p*-toluate moiety in **5** is involved in C–H···O hydrogen bonding with the hydrogen atom H7C of one of the methyl groups of 3,5-lutidine present in the inversion related adjacent molecule. The C–H···O hydrogen bonding in complexes **3** and **5** grows along *c*-axis and *a*-axis, respectively to afford a one-dimensional chain (see Figs. 6 and 8).

We have shown that less basic and sterically more hindered *o*-toluate in mononuclear complex **4** is coordinated to the zinc atom in monodentate coordination mode whereas more basic and sterically less hindered benzoate and *m*-toluate in dinuclear complexes **2** and **3** are coordinated to the zinc atom in syn–syn bidentate bridging coordination mode. The sterically less hindered and even more basic *p*-toluate in the mononuclear complex **5** is coordinated to the zinc atom in a chelating coordination mode. The shift of the carboxylate coordination mode from monodentate in **4** to syn–syn bidentate bridging in **2** and **3** and to the chelating in **5** implied largely the influence of basicity of the lone pair on the carbonyl oxygen of the carboxylate moiety and sterics. Such 'carboxylate shift' process has important implications for metalloenzymes in understanding their catalytic activities [51–54].

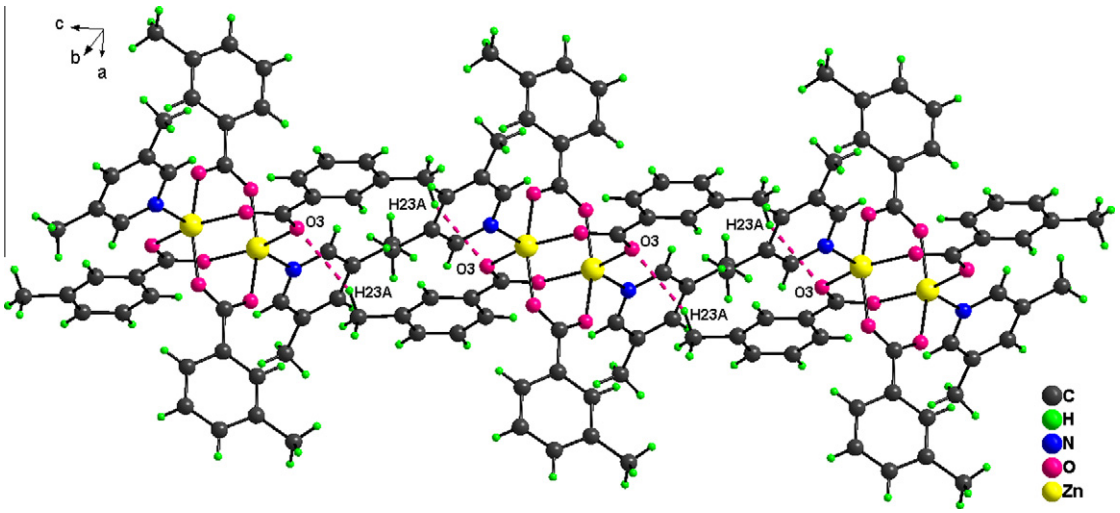

Fig. 6. Packing diagram of **3** illustrating a C–H···O hydrogen bonding in the crystal lattice. Hydrogen bond parameters, C23–H23A: 0.96 Å; H23A···O3: 2.68 Å, C23···O3: 3.60 Å, C23–H23A···O3: 158°.

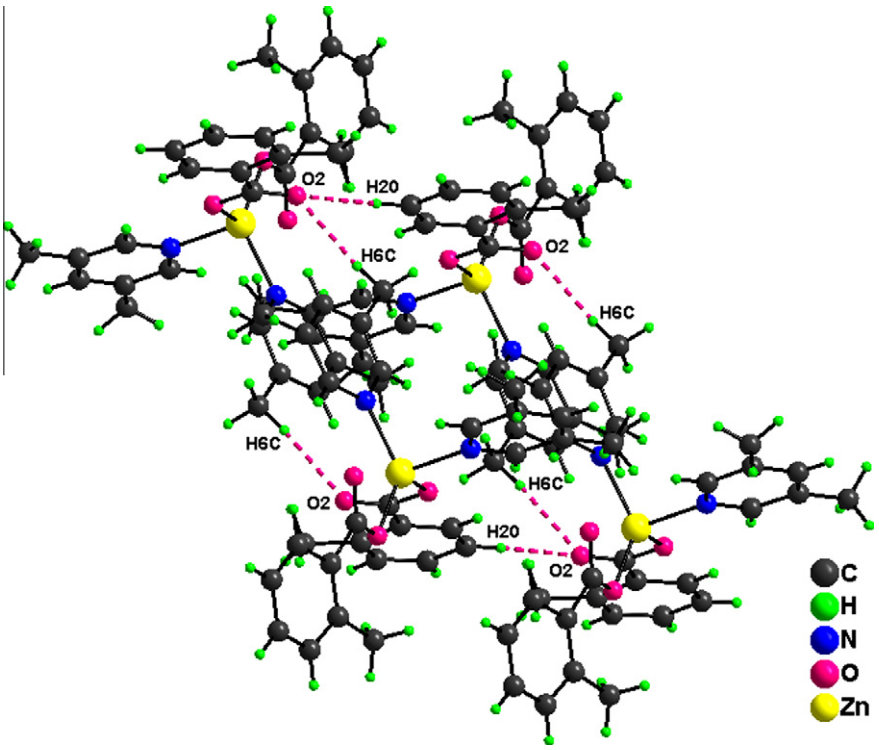

Fig. 7. Packing diagram of **4** illustrating a C–H···O hydrogen bonding in the crystal lattice. Hydrogen bond parameters, C20–H20: 0.93 Å; H20···O2: 2.64 Å, C20···O2: 3.52 Å, C20–H20···O2: 157° and C6–H6C: 0.96 Å; H6C···O2: 2.46 Å, C6···O2: 3.42 Å, C6–H6C···O2: 173°.

3.3. Spectroscopic studies

IR spectroscopy is one of the useful techniques to assign the carboxylate coordination modes and the following trend is generally accepted as a guideline to differentiate various carboxylate coordination modes [55–58].

$$\Delta v = v_{asym}(OCO) - v_{sym}(OCO)$$

$$\Delta v \text{ chelating} < \Delta v \text{ bridging} < \Delta v \text{ ionic} < \Delta v \text{ monodentate}$$

The Δv values obtained from IR data, and from X-ray diffraction data using Tasumi's equation (Eq. (1)) [59] for complexes **1**–**5** are listed in Table 3. The Δv values for the corresponding RC(O)OM (R = Me; M = Na [60] and R = C_6H_5, C_6H_4Me-2, C_6H_4Me-3 and C_6H_4Me-4; M = K [61]) are also included in Table 3 to unambiguously assign the carboxylate coordination modes in complexes **1**–**5**.

$$\Delta v_{calcd} = 1818.1\delta r + 16.47(\theta_{OCO} - 120) + 66.8 \quad (1)$$

In Eq. (1) δr is the difference between two C–O bond lengths (in Å) and θoco is the OCO angle (in °). Eq. (1) was applied by us [40] and others [58] to better interpret Δv values of several Lewis base coordinated zinc(II) carboxylate complexes bearing distinct carboxylate coordination modes. According to Eq. (1), the variation of 0.01 Å in δr or 1° in θoco gives rise to a change of 16–18 cm^{-1} in the value of Δv. Sometimes, a significant deviation was observed

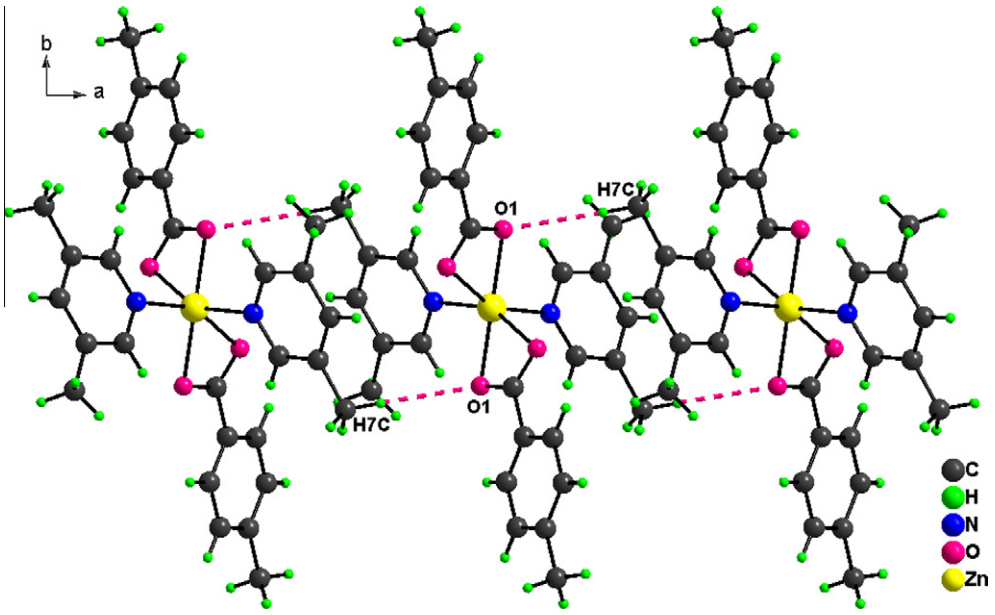

Fig. 8. Packing diagram of **5** illustrating a C–H···O hydrogen bonding in the crystal lattice. Hydrogen bond parameters, C7–H7C: 0.96 Å; H7C···O1: 2.68 Å, C7···O1: 3.62 Å, C7–H7C···O1: 167°.

Table 3
IR spectral data (cm^{-1}) of **1**–**5**.

	$\Delta\nu_{calcd}$ ($\Delta\nu_{exp}$)	$\Delta\nu$ for RC(O)OM	Coordination mode
1	234 (204)	164	monodentate (hydrogen bonded)
	233 (219)		monodentate
2	173 (182)	136	syn–syn bidentate bridging
	167 (168)		syn–syn bidentate bridging
3	157 (179)	170	syn–syn bidentate bridging
	193 (183)		syn–syn bidentate bridging
4	193 (200)	146	monodentate
	164 (160)		monodentate
5	98 (139)	145	chelating

Table 4
Solid state CP-MAS ^{13}C NMR data (ppm) for **1**–**5**.

	CH_3	Ar*C*	O*C*(O)
1	17.1, 18.3, 20.4, 25.0	134.9, 141.6, 145.3	176.6, 181.1
2	16.4	125.1, 127.6, 129.7, 131.0, 132.8, 135.5, 138.4, 142.1, 144.8	170.0, 171.6
3	15.6, 16.2, 20.0	125.9, 128.2, 129.9, 131.5, 133.4, 136.3, 138.4, 144.5	169.6, 171.6
4	17.2, 21.7, 24.2	125.7, 127.3, 132.5, 135.0, 141.0, 145.5	172.6, 175.6
5	16.6, 17.6, 20.8	126.0, 127.0, 128.6, 133.0, 143.0, 143.9	174.1

between the $\Delta\nu_{calcd}$ and $\Delta\nu_{exp}$ values due to the involvement of carbonyl oxygen in H-bonding [62] and also due to the cage deformation [40,58].

There is a fairly good agreement between $\Delta\nu_{calcd}$ and $\Delta\nu_{exp}$ values for one of the monodentate acetate coordination modes in **1**, both syn–syn bidentate bridging coordination modes in **2**, one of the syn–syn bidentate bridging coordination modes in **3**, and both monodentate carboxylate coordination modes in **4**. However, there is a significant deviation between Δ_{calcd} and Δ_{exp} values for one of the monodentate acetate coordination modes in **1**, one of the syn–syn bidentate bridging coordination modes in **3** and the chelating coordination mode in **5**. The aforementioned deviation may be ascribed to the presence of an intermolecular O–H···O/C–H···O hydrogen bonding interactions in the crystal lattice.

The solution ^1H and ^{13}C NMR spectral pattern of **1**–**5** appeared deceptively simple and less informative for the structural elucidation. This artifact could be due to sample dissociation or due to a rapid 'carboxylate shift' process that occurs on a time scale faster than NMR time scale [40,63]. The solid-state CP-MAS ^{13}C NMR was proven as a useful technique to distinguish various acetate coordination modes of zinc(II) acetate complexes [40,64,65]. Sometimes, even crystallographically different carbonyl carbons of the carboxylate moieties were distinguished with the aid of solid-state CP-MAS ^{13}C NMR data [65]. Hence, solid-state CP-MAS ^{13}C NMR data was recorded for **1**–**5** and the respective δ_C values are listed in Table 4.

The solid-state CP-MAS ^{13}C NMR spectrum of **1** revealed two peaks at δ_C = 176.6 and 181.1 ppm assignable to O*C*(O) carbon nuclei. The δ_C = 176.6 ppm value is assigned to the carbonyl carbon of the monodentate acetate [40,64] and the δ_C = 181.1 ppm value is assigned to the carbonyl carbon of the monodentate acetate

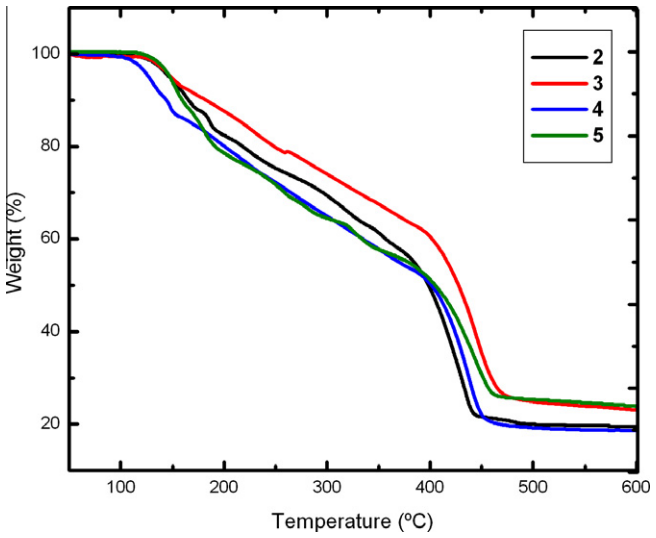

Fig. 9. Thermogravimetric traces of **2**–**5** in air.

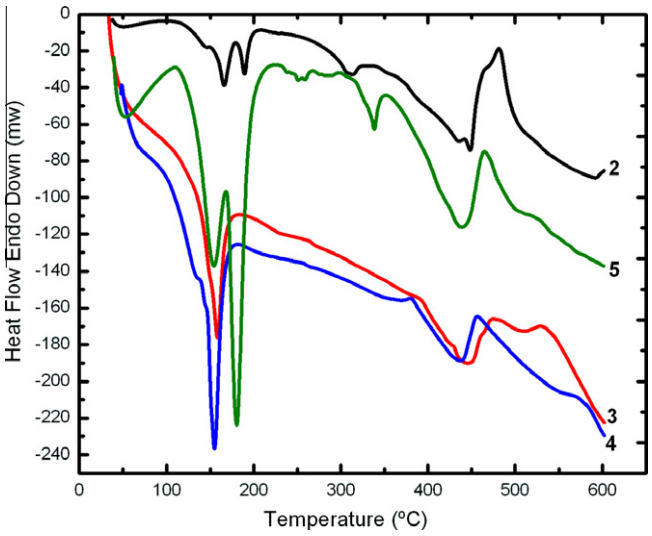

Fig. 10. Differential thermal analyses of **2**–**5** in air.

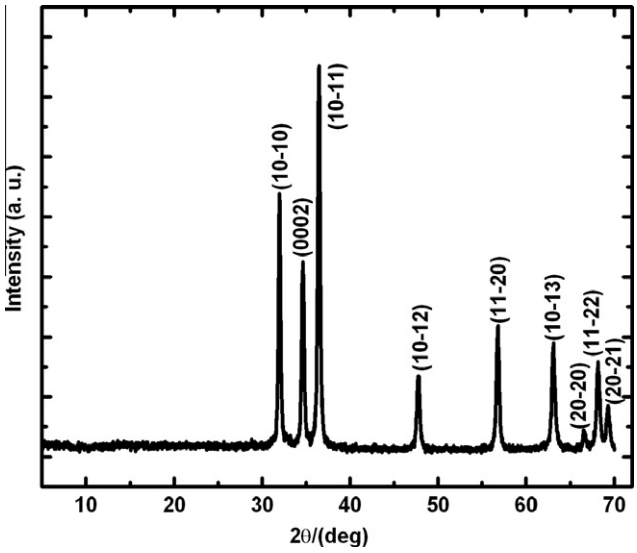

Fig. 11. PXRD pattern of ZnO obtained by calcination of **4** at 350 °C for 3 h in air.

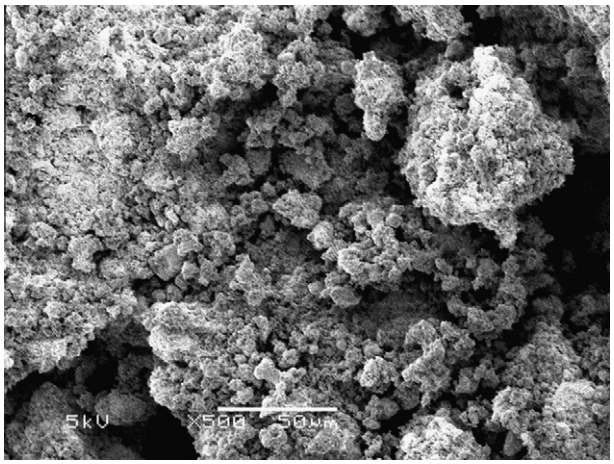

Fig. 12. SEM image of highly porous ZnO obtained after calcination of **4** at 350 °C for 3 h in air.

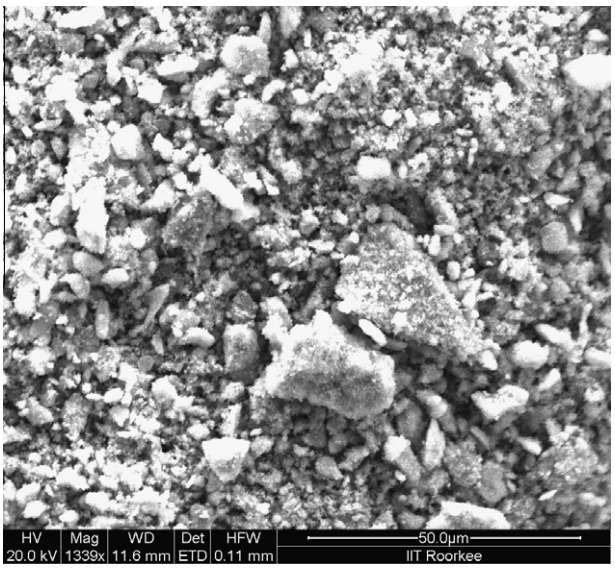

Fig. 13. SEM image of highly porous ZnO obtained after calcination of **4** at 450 °C for 6 h in air.

moiety which is hydrogen bonded to a water molecule. Interestingly, four types of ^{13}C NMR signals (δ_C = 17.1, 18.3, 20.4, and 25.0 ppm) were observed for CH_3 carbon of **1** indicating a chemical shift anisotropy of CH_3 carbon of two distinct 3,5-lutidine and acetate moieties and this observation is consistent with the structure found in the crystal lattice. Complexes **2**–**4** revealed two types of ^{13}C NMR signals whereas complex **5** revealed only one for the carbonyl carbon as the formerly mentioned complexes possess two crystallographically distinct carbonyl carbon whereas the latter possess only one.

Complexes **1**–**5** revealed a cluster of peaks centered at *m*/*z* = 398, 831, 886, 551, and 550 amu, respectively characteristic of $[M-H_2O+H]^+$ (**1**) and $[M+H]^+$ (**2**–**5**) moities due to different isotopes of zinc.

3.4. Thermal decomposition studies

The TGA of complex **1** indicated loss of a water molecule (experimental weight loss 4.25%; Theoretical weight loss: 4.33%) in 37–175 °C temperature range. No residue was left at the end of thermolysis event and this is likely due to the volatile nature of complex **1**. The TGA and DTA traces of **2**–**5** carried out in air are shown in Figs. 9 and 10, respectively. The TGA data of **2**–**5** indicated loss of 3,5-lutidine and CO_2 molecule in sequence as verified by weight loss calculations. The total weight loss corresponded to ZnO in each case as the decomposed product. Depending upon the nature of carboxylate moieties and nuclearity/carboxylate coordination modes present in **2**–**5**, different number of intermediates were observed in the TGA/DTA traces. The DTA traces revealed the weight losses to be exothermic. Complexes **2**–**5** were separately calcined at 350 °C for 3 h in air that yielded thermodynamically stable hexagonal form of ZnO as deduced from the PXRD pattern. The observed PXRD pattern matched well with the authentic ZnO (ICSD-067454) in each case. As a representative example, PXRD pattern and SEM image for ZnO obtained from the decomposition of **4** are presented in Figs. 11 and 12, respectively. The porous nature of ZnO shown in the SEM image may be ascribed to the huge amount of CO_2 evolved during thermolysis event as hypothesized in the thermogravimetric traces. However, ZnO obtained from the aforementioned experimental condition was dirty white in color possibly arising due to incomplete

combustion. On heating the complex **4** at 450 °C for 6 h in air resulted in off-white ZnO indicating the complete removal of carbon. The morphology of ZnO was different under this condition as observed from the SEM image shown in Fig. 13.

4. Concluding remarks

The mononuclear complex **1** and four 3,5-lutidine coordinated zinc(II) aryl carboxylate complexes (**2**–**5**) were synthesized in high yield and structurally characterized. Complex **1** possesses two distinct acetate and 3,5-lutidine moieties as one of the acetates forms an intermolecular O–H···O hydrogen bonding with a lattice water molecule as revealed by X-ray diffraction data and further supported by solid-state CP-MAS ^{13}C NMR data. Complexes **2** and **3** possess a paddlewheel framework, whereas complexes **4** and **5** possess a mononuclear framework with the zinc atom in tetrahedral and an octahedral geometry, respectively. It was observed that subtle basic/steric properties of the carboxylate moieties influence their coordination modes which in turn influence the nuclearity of the products. As basicity of the carbonyl oxygen of the carboxylate moiety increases in complexes **2**–**5**, its tendency to coordinate with the Zn center also increases. Hence, the carboxylate coordination mode shifts from the monodentate in **4** to syn–syn bidentate bridging in **2** and **3** and to the chelating in **5**. The solid-state CP-MAS ^{13}C NMR data was shown to be a useful technique to distinguish even the crystallographically different O*C*(O) carbon in complexes **2**–**5**. The thermal decomposition study of **2**–**5** demonstrated the use of these complexes to be potential precursors for ZnO in conjunction with PXRD pattern and SEM images.

Acknowledgments

The authors acknowledge Council of Scientific and Industrial Research, New Delhi (# 01/(2076)/06 EMR-II) for financial support and for a fellowship (U.K.). NMR Research center, Indian Institute of Science, Bangalore 560012 and Department of Chemistry, Indian Institute of Technology Kanpur, Kanpur 208016 are acknowledged for the solid-state CP-MAS ^{13}C NMR data for all complexes reported in this manuscript and crystallographic data for complex **1**, respectively.

Appendix A. Supplementary material

CCDC 808869, 750049, 750051, 750050, and 750048 contain the supplementary crystallographic data for compounds **1**, **2**, **3**, **4** and **5**, respectively. These data can be obtained free of charge from The Cambridge Crystallographic Data Centre via www.ccdc.cam.ac.uk/data_request/cif. Supplementary data associated with this article can be found, in the online version, at doi:10.1016/j.ica.2011.01.083.

References

[1] Ü. Özgur, Y.I. Alivov, C. Liu, A. Teke, M.A. Reshchikov, S. Doğan, V. Avrutin, S.-J. Cho, H. Morkoc, J. Appl. Phys. 98 (2005) 041301.
[2] S.J. Pearton, D.P. Norton, K. Ip, Y.W. Heo, T. Steiner, Prog. Mater. Sci. 50 (2005) 293.
[3] D.W. Bahnemann, C. Kormann, M.R. Hoffmann, J. Phys. Chem. 91 (1987) 3789.
[4] L. Spanhel, M.A. Anderson, J. Am. Chem. Soc. 113 (1991) 2826.
[5] Y. Inubushi, R. Takami, M. Iwasaki, H. Tada, S. Ito, J. Colloid Interface Sci. 200 (1998) 220.
[6] S.A. Studenikin, N. Golego, M. Cocivera, J. Appl. Phys. 83 (1998) 2104.
[7] N. Audebrand, J.-P. Auffrédic, D. Louër, Chem. Mater. 10 (1998) 2450.
[8] W. Wieldraaijer, J. van Balen Blanken, E.W. Kuipers, J. Cryst. Growth 126 (1993) 305.
[9] I. Alessandri, M. Zucca, M. Ferroni, E. Bontempi, L.E. Depero, Cryst. Growth Des. 9 (2009) 1258.
[10] D.C. Kim, J.H. Lee, H.K. Cho, J.H. Kim, J.Y. Lee, Cryst. Growth Des. 10 (2010) 321.
[11] M.L. Kahn, M. Monge, V. Collière, F. Senocq, A. Maisonnat, B. Chaudret, Adv. Funct. Mater. 15 (2005) 458.
[12] K. Black, A.C. Jones, I. Alexandrou, P.N. Heys, P.R. Chalker, Nanotechnology 21 (2010) 045701.
[13] D. Bekermann, D. Rogalla, H.-W. Becker, M. Winter, R.A. Fischer, A. Devi, Eur. J. Inorg. Chem. (2010) 1366.
[14] J.S. Matthews, O.O. Onakoya, T.S. Ouattara, R.J. Butcher, Dalton Trans. (2006) 3806.
[15] M. Hamid, A.A. Tahir, M. Mazhar, F. Ahmad, K.C. Molloy, G. Kociok-Kohn, Inorg. Chim. Acta 361 (2008) 188.
[16] A. Cingolani, S. Galli, N. Masciocchi, L. Pandolfo, C. Pettinari, A. Sironi, Dalton Trans. (2006) 2479.
[17] V. Zeleňák, M. Sabo, W. Massa, P. Llewellyn, Inorg. Chim. Acta 357 (2004) 2049.
[18] W. Maret, Y. Li, Chem. Rev. 109 (2009) 4682.
[19] J. Weston, Chem. Rev. 105 (2005) 2151.
[20] G. Parkin, Chem. Rev. 104 (2004) 699.
[21] W.N. Lipscomb, N. Sträter, Chem. Rev. 96 (1996) 2375.
[22] D.E. Wilcox, Chem. Rev. 96 (1996) 2435.
[23] B.L. Vallee, D.S. Auld, Acc. Chem. Res. 26 (1993) 543.
[24] D.J. Darensbourg, Chem. Rev. 107 (2007) 2388.
[25] G.W. Coates, D.R. Moore, Angew. Chem., Int. Ed. 43 (2004) 6618.
[26] D.J. Darensbourg, J.R. Wildeson, J.C. Yarbrough, Inorg. Chem. 41 (2002) 973.
[27] D.J. Tranchemontagne, J.L. Mendoza-Cortés, M. O'Keeffe, O.M. Yaghi, Chem. Soc. Rev. 38 (2009) 1257.
[28] B.S. Luisi, Z. Ma, B. Moulton, J. Chem. Crystallogr. 37 (2007) 743.
[29] S.I. Vagin, A.K. Ott, B. Rieger, Chem. Ing. Tech. 79 (2007) 767.
[30] N.L. Toh, M. Nagarathinam, J.J. Vittal, Angew. Chem., Int. Ed. 44 (2005) 2237.
[31] O.M. Yaghi, M. O'Keeffe, N.W. Ockwig, H.K. Chae, M. Eddaoudi, J. Kim, Nature 423 (2003) 705.
[32] M. Eddaoudi, D.B. Moler, H. Li, B. Chen, T.M. Reineke, M. O'Keeffe, O.M. Yaghi, Acc. Chem. Res. 34 (2001) 319.
[33] M. Eddaoudi, H. Li, T. Reineke, M. Fehr, D. Kelley, T.L. Groy, O.M. Yaghi, Top. Catal. 9 (1999) 105.
[34] P. Hubberstey, K. Lin, N.R. Champness, M. Schröder, in: L. MacGillivray (Ed.), Metal–Organic Frameworks: Design and Application, John Wiley and Sons, Inc., Hoboken, NJ, USA, 2010, pp. 131–164 (Chapter 4).
[35] A. Karmakar, R.J. Sarma, J.B. Baruah, Inorg. Chem. Commun. 9 (2006) 1169.
[36] V. Zeleňák, I. Císařová, P. Llewellyn, Inorg. Chem. Commun. 10 (2007) 27.
[37] A. Karmakar, J.B. Baruah, Polyhedron 27 (2008) 3409.
[38] H. Kwak, S.H. Lee, S.H. Kim, Y.M. Lee, B.K. Park, E.Y. Lee, Y.J. Lee, C. Kim, S.-J. Kim, Y. Kim, Polyhedron 27 (2008) 3484.
[39] K.F. Konidaris, M. Kaplanis, C.P. Raptopoulou, S.P. Perlepes, E. Manessi-Zoupa, E. Katsoulakou, Polyhedron 28 (2009) 3243.
[40] U. Kumar, J. Thomas, N. Thirupathi, Inorg. Chem. 49 (2010) 62.
[41] U. Kumar, J. Thomas, M. Agarwal, N. Thirupathi, Inorg. Chim. Acta (2011), doi:10.1016/j.ica.2011.01.040.
[42] SMART, Bruker Molecular Analysis Research Tool, Version 5.0, Bruker Analytical X-ray Systems, Madison, WI, 2000.
[43] SAINT-NT, Version 6.04, Bruker Analytical X-ray Systems, Madison, WI, 2001.
[44] G.M. Sheldrick, SHELXTL-NT, Version 6.12, Reference Manual.
[45] B. Klaus, DIAMOND, Version 2.0 c, University of Bonn, Bonn, Germany, 2004.
[46] D.R. Lide (Ed.), CRC Handbook of Chemistry and Physics, 81st ed., CRC Press, New York, 2000/2001 (Sec. 8).
[47] B. Singh, J.R. Long, F. Fabrizi de Biani, D. Gatteschi, P. Stavropoulos, J. Am. Chem. Soc. 119 (1997) 7030.
[48] Y.B. Koh, G.G. Christoph, Inorg. Chem. 18 (1979) 1122.
[49] H. Nacefoglu, W. Clegg, A.J. Scott, Acta Crystallogr., Sect. E: Struct. Rep. Online 58 (2002) m121.
[50] V. Zeleňák, M. Sabo, W. Massa, J. Cernak, Acta Crystallogr., Sect. C: Cryst. Struct. Commun. 60 (2004) m85.
[51] R.L. Rardin, W.B. Tolman, S.J. Lippard, New J. Chem. 15 (1991) 417.
[52] D.D. LeCloux, A.M. Barrios, T.J. Mizoguchi, S.J. Lippard, J. Am. Chem. Soc. 120 (1998) 9001.
[53] S.F. Sousa, P.A. Fernandes, M.J. Ramos, J. Am. Chem. Soc. 129 (2007) 1378.
[54] M. Torrent, D.G. Musaev, K. Morokuma, J. Phys. Chem. B 105 (2001) 322.
[55] R.C. Mehrotra, R. Bohra, Metal Carboxylates, Academic Press, New York, 1983.
[56] G.B. Deacon, R.J. Phillips, Coord. Chem. Rev. 33 (1980) 227.
[57] K. Nakamoto (Ed.), Infra-red and Raman Spectra of Inorganic and Coordination Compounds, Wiley, New York, 1997.
[58] V. Zeleňák, Z. Vargová, K. Györyová, Spectrochim. Acta Part A 66 (2007) 262.
[59] M. Nara, H. Torii, M. Tasumi, J. Phys. Chem. 100 (1996) 19812.
[60] K. Ito, H.J. Bernstein, Can. J. Chem. 34 (1956) 170.
[61] J.F. Arenas, S. Montero, J. Morcillo, J.L. Núñez, An. Quim. 69 (1973) 311.
[62] T. Ishioka, Y. Shibata, M. Takahashi, I. Kanesaka, Y. Kitagawa, K.T. Nakamura, Spectrochim. Acta Part A 54 (1998) 1827.
[63] A. Demšar, J. Košmrlj, S. Petriček, J. Am. Chem. Soc. 124 (2002) 3951.
[64] B.-H. Ye, X.-Y. Li, I.D. Williams, X.-M. Chen, Inorg. Chem. 41 (2002) 6426.
[65] P.A. Hunt, B.P. Straughan, A.A.M. Ali, R.K. Harris, B.J. Say, J. Chem. Soc., Dalton Trans. (1990) 2131.